Nanotopographical Effects on Mesenchymal Stem Cell Morphology and Phenotype

Penelope Tsimbouri,[1]* Nikolaj Gadegaard,[2] Karl Burgess,[3] Kate White,[4] Paul Reynolds,[2] Pawel Herzyk,[5] Richard Oreffo,[4,6] and Matthew J. Dalby[1]

[1]Centre for Cell Engineering, Institute of Molecular, Cell and Systems Biology, College of Medical, Veterinary and Life Sciences, Joseph Black Building, University of Glasgow, Glasgow G12 8QQ, Scotland, UK

[2]Division of Biomedical Engineering, School of Engineering, University of Glasgow, Glasgow G12 8LT, Scotland, UK

[3]Glasgow Polyomics Facility, Joseph Black Building, Institute of Biomedical and Life Sciences, University of Glasgow, Glasgow G12 8QQ, Scotland, UK

[4]Bone & Joint Research Group, Centre for Human Development, Stem Cells and Regeneration, Institute of Developmental Sciences, University of Southampton, Southampton SO16 6YD, UK

[5]Sir Henry Wellcome Functional Genomics Facility, College of Medical, Veterinary and Life Sciences, Joseph Black Building, University of Glasgow, G12 8QQ, UK

[6]Stem Cell Unit, Department of Anatomy, College of Medicine, King Saud University, Riyadh, Kingdom of Saudi Arabia

ABSTRACT

There is a rapidly growing body of literature on the effects of topography and critically, nanotopography on cell adhesion, apoptosis and differentiation. Understanding the effects of nanotopography on cell adhesion and morphology and the consequences of cell shape changes in the nucleus, and consequently, gene expression offers new approaches to the elucidation and potential control of stem cell differentiation. In the current study we have used molecular approaches in combination with immunohistology and transcript analysis to understand the role of nanotopography on mesenchymal stem cell morphology and phenotype. Results demonstrate large changes in cell adhesion, nucleus and lamin morphologies in response to the different nanotopographies. Furthermore, these changes relate to alterations in packing of chromosome territories within the interphase nucleus. This, in turn, leads to changes in transcription factor activity and functional (phenotypical) signalling including cell metabolism. Nanotopography provides a useful, non-invasive tool for studying cellular mechanotransduction, gene and protein expression patterns, through effects on cell morphology. The different nanotopographies examined, result in different morphological changes in the cyto- and nucleo-skeleton. We propose that both indirect (biochemical) and direct (mechanical) signalling are important in these early stages of regulating stem cell fate as a consequence of altered metabolic changes and altered phenotype. The current studies provide new insight on cell–surface interactions and enhance our understanding of the modulation of stem cell differentiation with significant potential application in regenerative medicine. J. Cell. Biochem. 115: 380–390, 2014. © 2013 Wiley Periodicals, Inc.

Current advances in the understanding of cell response to nanotopography provide us with new directions in the field of regenerative medicine [Dalby et al., 2007; McMurray et al., 2011; McNamara et al., 2011]. Important results have included influence of targeted osteogenesis of mesenchymal stem cells (MSCs) indicating that implant modifications could improve clinical outcome [Dalby et al., 2007; Park et al., 2007; Oh et al., 2009; McNamara et al., 2011].

Furthermore, it was recently shown that nanostructured surfaces can retain MSC phenotype and maintain stem cell growth with implications therein for provision of high quality stem cells to clinic [McMurray et al., 2011]. Furthermore, Chen and co-workers, and Ji and coworkers have recently demonstrated the potential for modifying embryonic stem cell response using nanotopographical cues [Chen et al., 2012; Ji et al., 2012].

In order to understand stem cell differentiation it is critical to have a good understanding of the mechanisms of the physiological processes that control cell-biomaterial interactions and the influence of nanotopography on cell adhesion and phenotype. In this study we have used bone marrow-derived MSCs (more correctly described as skeletal stem cells) to examine nanotopographical cues on phenotype. MSCs can differentiate into different cell types including chondrocytes [Muraglia et al., 2000], smooth muscle cells [Engler et al., 2006; Narita et al., 2008], osteoblasts, adipocytes [Pittenger et al., 1999], neural cells [Yim et al., 2007] and fibroblasts. While differentiation may affect the cell shape, recent studies have shown that changes in cell shape can alter the differentiation of pre-committed mesenchymal lineages [McBeath et al., 2004; Treiser et al., 2010]. Intracellular tension has been implicated in directing stem cell differentiation; a high-tension state inducing osteogenic differentiation, while a low-tension state induces adipogenic differentiation [Thomas et al., 2002; McBeath et al., 2004; Kilian et al., 2010]. Furthermore, recent developments indicate the necessity of an intermediate level of cellular tension for stem cell self-renewal [Gilbert et al., 2010; Tsimbouri et al., 2012].

Interactions between stem cells and the extracellular matrix (ECM) lead to indirect or direct effects on cells, known as mechanotransduction, with concomitant changes in gene expression. Indirect mechanotransduction comprises the canonical biochemical signalling cascades resulting from for example integrin binding and focal adhesion formation [Wang et al., 1993]. However, direct mechanotransduction arises as a result of conformational changes in the cell cytoskeleton, forming direct links between the ECM and the cell nucleus through the nucleoskeletal lamins (the nuclear intermediate filaments) and possibly to the chromosomes themselves via telomeric chromatin/lamin interactions [Wang et al., 1993; Ingber, 1997].

The nucleoskeleton consists of a network of proteins consisting of lamins A and C [Lin and Worman, 1993] B1 [Lin and Worman, 1995] and B2 [Biamonti et al., 1992] in most somatic cell types. The lamina is responsible for the structural support of the nucleus. The lamina forms part of the link to the cytoskeleton providing the correct nuclear and centrosomal organization [Gehrig et al., 2008]. Furthermore, the lamina is associated with DNA replication; lamin B foci are linked with proliferating cell nuclear antigen (PCNA), a protein facilitating DNA replication through DNA polymerase δ in eukaryotic cells [Moir et al., 1994, 2000].

A few studies have shown that actively differentiating cells have a rapid metabolism whereas less differentiated cells, including stem cells, are metabolically quiescent. Yanes and coworkers showed that ESCs in pluripotent state contained a high proportion of metabolites with chemical unsaturations (e.g. CC bonds) [Yanes et al., 2010]. When the cells were stimulated to undergo active differentiation, the metabolite profile shifted to one of a majority of saturated metabolites. The authors hypothesised that the chemical saturations allow chemical plasticity in the stem cells and allowed the cells to mediate differentiation through regulation of redox status and activation of oxidative pathways. Preliminary evidence has also indicated that MSCs may also have greater proportions of unsaturations in their self-renewing state and that they loose these with differentiation and also that general metabolism increases with for example osteogenesis [Yanes et al., 2010].

To enhance our understanding of mechanotransduction in stem cell differentiation and metabolism, two nanotopographies have been used in this report (Fig. 1A). Firstly, a surface that promotes high intracellular tension and osteogenesis (near square 50, NSQ50) [Dalby et al., 2007] and a self-renewal promoting surface (square, SQ) [McMurray et al., 2011]. The topographies consist of nanopits of 120 nm in diameter, 100 nm in depth arranged in a square lattice. For the SQ, the centre–centre spacing of the pits is 300 nm, for the NSQ50, each pit has up to a 50 nm offset in X and Y.

The architectural and molecular effects of these nanotopographies were investigated at the cellular level using focal adhesion characterisation and cell feature image analysis; at the nuclear level by lamin immunostaining; at the mRNA level using Affymetrix arrays to look at canonical pathways relevant to MSC phenotypes; and finally the metabolomics level as the functional readout of cell physiology. We demonstrate that as phenotype was retained or differentiation initiated, the nuclear lamina was remodelled, with concomitant modulation of gene expression and metabolic changes within the skeletal stem and progenitor cell populations.

MATERIALS AND METHODS

ELECTRON BEAM LITHOGRAPHY

The substrates used in this study were made using electron beam lithography [Gadegaard et al., 2003] nickel die fabrication and hot embossing using an injection moulder. To briefly describe the process, the master substrates were fabricated to form an array of 120 nm diameter pits of 100 nm depth and 300 nm pitch in a square (SQ) arrangement. The NSQ50 substrates had a controlled disorder by changing the pits from perfectly square (SQ) by ±50 nm and maintaining an average 300 nm pitch (Fig. 1A scanning electron microscopy (SEM) images). Nickel dies were made directly from the patterned resist samples. This was followed by the addition of a thin layer (50 nm) of Ni–V was sputter coated on the samples, acting as an electrode in the subsequent electroplating process. The nickel shims were then cleaned using chloroform for 15 min in an ultrasound bath. The silicon residue was then stripped by wet etching in 25% KOH at 80°C for 1 h which followed by rinsing thoroughly in ROH$_2$O and air-drying. An injection moulder was used to make replicates of the shims.

CELL EXTRACTION AND CULTURE

MSCs were derived from human bone marrow (from a large number of patients), using the Stro-1 antibody and magnetic activated cell sorting (MACS) as previously described [Biggs et al., 2007]. MSCs were maintained in basal media (aMEM (PAA) supplemented with 10% FBS (PAA), 1% (v/v) 200 mM L-glutamine (Gibco) and antibiotics (6.74 U/ml penicillin–streptomycin, 0.2 μg/ml Fungizone, Gibco)) at 37°C with 5% CO$_2$ in a humidified incubator. MSCs′ density onto the materials was 1×10^4 cells/ml and cultured for 3 days. Cells were always used at passages P1–P2.

LDL BLOCK

After counting the cells using a haemocytometer, the required number of cells were blocked by adding 1:1 volume of antibody LDL (Epitomics) to the cell pellet. MSCs were seeded onto the material surfaces at 1×10^4 cells/ml and the LDL antibody was added [1:2,000 dilution in the culture medium; Wood et al., 2008].
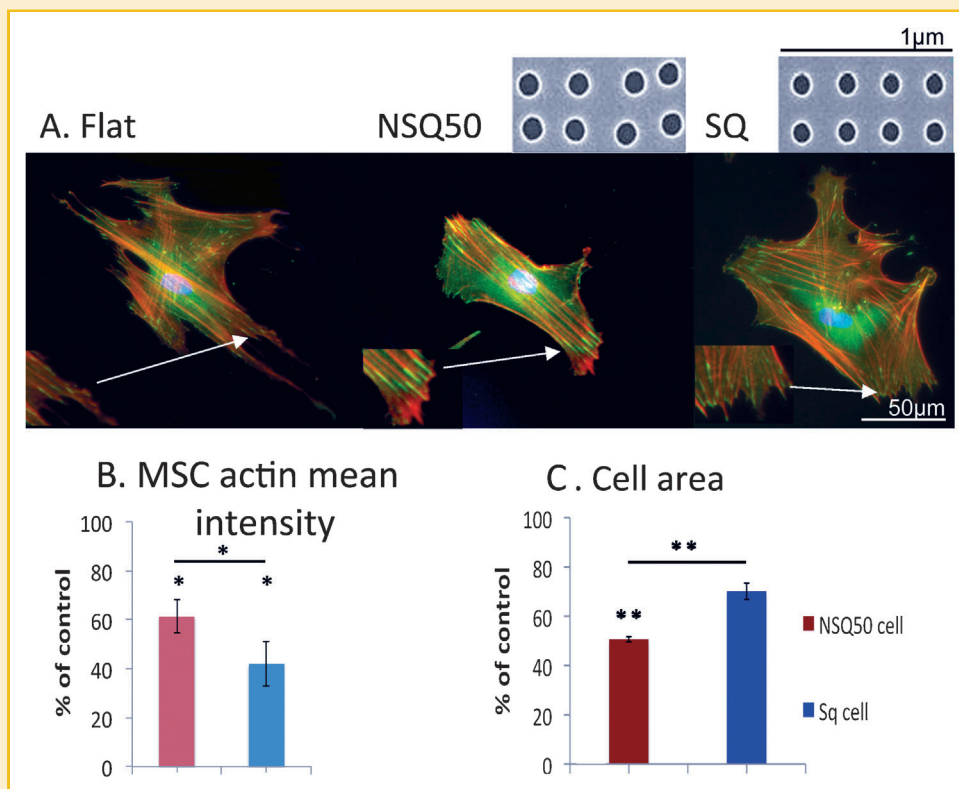
Fig. 1. Fluorescent microscopy images of MSC morphology and attachment on nanopit substrates. A: Flat control substrate, MSCs displayed a spread morphology with numerous adhesions. On NSQ50 substrate (SEM), MSCs were spread with large lamellae and displayed an elongated cell shape. Cells were observed to develop stress fibres with significantly longer adhesions than SQ (SEM; $P < 0.05$). On SQ, cells displayed reduced spread morphology and adopted a stellate shape with fewer stress fibres and adhesions. Green, vinculin; red, actin; blue, nucleus. B: Graph shows actin mean intensity $\pm$ SD as % of control. Comparison was done by ANOVA $^*P < 0.05$, $^{**}P < 0.01$, $^{***}P < 0.001$, n = 268. C: Graph shows mean cell area $\pm$ SD as % of control. Comparison was done by ANOVA $^*P < 0.05$, $^{**}P < 0.01$, $^{***}P < 0.001$, n = 40. Note: markings above the error bars denote comparison to flat control; comparison between SQ and NSQ50 is denoted by a line. Scale bar as indicated.

JNK INHIBITION

MSCs seeded onto the material surfaces at 1×10^4 cells/ml. The 420119 Jun kinase (JNK) Inhibitor II (MERCK) was used at a final concentration of 25 µM for 3 days, which was followed by a 7-day recovery period.

CYTOSKELETAL POISONING

The MSCs seeded onto the materials at 1×10^4 cells/ml, were cultured in basal media supplemented with blebbistatin, a non-muscle myosin II inhibitor (50 µM) for 3 days.

IMMUNOFLUORESCENCE

MSCs were fixed (10% formaldehyde solution), permeabilised, blocked in 1% (w/v) BSA/1× PBS and stained with 1:50 anti-vimentin (Sigma), 1:150 for anti-vinculin (clone hVin-1, Sigma) or 1:100 p-myosin light chain (Cell Signalling, Phospho Ser 19), in 1% (w/v) BSA/PBS and incubated at 37°C for 1 h, (in conjunction with phalloidin-rhodamine 1:500 (Molecular Probes). In each experiment, two replicas of each nanotopography (NSQ50, SQ, FLAT) were stained. Cells were washed 3 × 5 min (1× PBS/0.5% Tween-20), an appropriate biotinylated secondary antibody (Vector Laboratories) was added at 1:50 in 1% (w/v) BSA/PBS and incubated again at 37°C for 1 h. After washing, FITC-conjugated streptavidin (1:50, Vector Laboratories) added to the samples and incubated for 30 min at 4°C followed by washing and mounting using Vectashield mountant with DAPI nuclear stain (Vector Laboratories).

CELLPROFILER

Image processing was performed using the CellProfiler software suite (Broad Institute, USA). Over 300 images were acquired using an upright fluorescence microscope (Olympus model BX51TF). An image processing pipeline was generated to load the DNA (DAPI), actin (rhodamine-phalloidin) and antibody conjugate fluorescein (FITC) for each image set; this was followed by automated detection of cell nuclei, cell morphology and marker staining intensity [Kamentsky et al., 2011].

ADHESION IMAGE ANALYSIS

Focal adhesion (FA) measurements were taken using the method described in [Biggs et al., 2008]. Approximately 50 cell images per substrate were exported to Adobe Photoshop and adhesion complexes marked with a three pixel wide straight line on an overlay of background image creating an adhesion schematic. ImageJ was used to analyse individual adhesions (60–400 per cell). The criteria for cell adhesion classification were set according to size restrictions described before [Wozniak et al., 2004; Diener et al., 2005]. Data

were sorted and analysed in Prism version 4.0c (GraphPad Software, San Diego, CA) using the Kruskal–Wallis one-way analysis of variance on ranks, which compared like subtypes. Results of $P < 0.05$ were considered significant (differences of $P < 0.05$ denoted by asterisk).

IMMUNOFLUORESCENCE FOR LAMINS

Following 3 days in culture, MSCs were fixed for 2 min in cold ($-20°$ C) methanol. The cells were then washed $3\times$ in $1\times$ PBS and blocked for 1 h in 3% (w/v) BSA/PBS at 37°C. Immunostaining was then performed as previously described in [Dalby et al., 2002]. In brief, following blocking, mouse anti-lamin A/C (1:50 in 1% (w/v) BSA/PBS; clone JOL3, Insight Biotech), or anti-lamin B1 (1:50 in 1% (w/v) BSA/PBS; clone 101-B7, Calbiochem) antibodies added and incubated at 37°C for 1 h. Following washing, an appropriate biotinylated secondary antibody (Vector Laboratories) was added at 1:50 in 1% (w/v) BSA/PBS and incubated at 37°C for 1 h. After washing, the samples were incubated with FITC-conjugated streptavidin (1:50, Vector Laboratories) for 30 min at 4°C. Finally, the samples were washed and mounted using Vectashield mountant with DAPI nuclear stain (Vector Laboratories).

FLUORESCENCE IN SITU HYBRIDISATION (FISH)

MSCs seeded onto the nanotopographies were fixed in 3:1 methanol/acetic acid for 30 min at room temperature. Samples were then rinsed in $2\times$ saline sodium citrate (SSC; 3 M NaCl, 0.3 M *tri*-sodium citrate, pH 7.4) for 3 h at 37°C. Biotinylated human chromosome 1 paint (Cambio, Cambridge, UK) was denatured at 65°C for 10 min and then incubated at 37°C for 30 min. The samples were then rinsed in H_2O for 30 s and dehydrated through a 70%, 90%, 90% (v/v) ethanol series, 2 min incubation each step, followed by a 5 min dehydration step in neat ethanol. After air-drying for 1 min, the samples were incubated at 65°C for 2 min in denaturation solution (7:1 formamide: $2\times$ SSC buffer). The samples were quenched again through an ice-cold ethanol series as described above and air-dried for 1 min. The denatured probe (10 µl) was added to each sample. To prevent evaporation of the probe, the samples were covered with pre-cut to shape and size parafilm and incubated in a humidified chamber for 42 h at 37°C. The samples were then rinsed in 45°C pre-warmed $1\times$ SSC buffer for 5 min followed by 2×5 min washes in stringency wash solution (1:1, $1\times$ SSC: formamide). The probe was detected using the Biotin Painting Kit (Cambio), according to the manufacturer's protocol. Triplicates of each nano-topography, were used in each experiment.

TERRITORY ANALYSIS

Image J (version 1.34s; Rasband, W.S., Image J, U.S. National Institutes of Health – http://rsb.info.nih.gov/ij/) was used to measure the distances from the nearest edge of the nuclei to the centres of the chromosomal territories. Statistical analysis was performed using Prism (GraphPad at www.graphpad.com/prism) and the Tukey–Kramer multiple comparisons post-test analysis of variance (ANOVA).

AFFYMETRIX ARRAYS

MSCs were cultured on the topographies for 3 days with 4 material replicates/biological replica for each nanotopography. The cells were washed in $1\times$ PBS and then lysed to obtain total RNA extracted using a Qiagen RNeasy minikit (Qiagen, UK). Gene expression changes were detected by hybridisation of mRNA to Affymetrix HuGene 1.0 ST human arrays as per manufacturers instructions. The bioinformatics analysis was initially based on rank product. To facilitate the identification of canonical signalling pathways and functional pathways and as well as to produce networks of our data, we applied a false discovery rate of 20% to upload selected gene changes to the Ingenuity Pathway Analysis (IPA) server. Statistics for functional analysis were carried out by Fischer's exact test (automatically performed by the software).

QUANTITATIVE REAL–TIME (Q)PCR

MSCs were cultured on the nano-topographies at a density of 1×10^4 cells/ml for 3 days. Total RNA was extracted using a Qiagen RNeasy micro kit according to the manufacturer's instructions. Real-time qPCR was carried out and analysed as previously described to assess the expression of RUNX2 (primer sequences: F-CAGACCAG-CAGCACTCCATA, R-ATCCCACAGCCCACAGTAAC) and SOX9 (primer sequences: F-AGACAGCCCCCTATCGACTT, R-CGGCAGG-TACTGGTCAAACT). RNA samples were reverse transcribed using the Quantitect reverse transcription kit (Qiagen). Real-time qPCR was carried out using the Applied Biosystems 7500 real-time PCR system. GapDH (primer sequences: F-GTCAGTGGTGGACCTGACCT, R-AC-CTGGTGCTCAGTGTAGCC) served as the housekeeping gene to normalize expression for the genes of interest. Primer sequences for the genes were validated by dissociation curve/melt curve analysis.

METABOLOMICS

MSCs were cultured on the nano-topographies at a density of 1×10^4 cells/ml for 3 days. Cells were first washed in cold $1\times$ PBS with the samples being kept cold at all times on a bed of ice. Metabolites were extracted using a 1:3:1 chloroform/methanol/water extraction buffer and placed on a shaking platform for 1 h at 4° C. The sample supernatant was transferred into 1.5 ml tubes and centrifuged for 3 min at 13,000g at 4°C. The samples were used for hydrophilic interaction liquid chromatography-mass spectrometry (UltiMate 3000 RSLC (Thermo Fisher) with a 150×4.6 mm ZIC-HILIC column running at 300 µl/min and Orbitrap Exactive (Thermo Fisher), respectively) analysis. After Nanodrop (Thermo Fisher) measurement, total protein content was found identical in all samples, thus no further standardization was necessary. A standard pipeline, consisting of XCMS [Smith et al., 2006] (peak picking), MzMatch [Scheltema et al., 2011] (filtering and grouping), and IDEOM [Creek et al., 2012] (further filtering, post-processing and identification) was used to process the raw mass spectrometry data. Identified core metabolites were validated against a panel of unambiguous standards by mass and retention time. Further putative identifications were allotted by mass and predicted retention time [Creek et al., 2011]. Means and standard errors of the mean were generated for every group of picked peaks and the resulting metabolomics data were uploaded to IPA software for metabolite pathway analysis.

Nine material replicates were used. Statistical analysis was carried out using the Tukey–Kramer multiple-comparisons post-test analysis of variance (ANOVA) as indicated in the figure legends.

RESULTS AND DISCUSSION

MSC MORPHOLOGY AND CYTOSKELETAL ORGANISATION

MSC morphology was dependent upon nanotopography as shown in Figure 1A. On the Flat control surface, MSCs displayed a well-spread phenotype with cytoplasmic processes. On the highly ordered SQ surface, MSCs were again well spread but with more stellate morphology. However, MSCs on the NSQ50 displayed a less spread morphology. Furthermore, MSCs on all materials formed contractile stress fibres but with notably more in cells on NSQ50 (Fig. 1B). Cell area measurements indicated that cells grown on the NSQ50 are significantly smaller in size ($P < 0.01$) from cells grown on either the Flat or the SQ topographies as shown in Figure 1C. Cell perimeter measurements support this observation further with MSCs on NSQ50 displaying the smallest perimeter in comparison to those grown on the SQ and Flat control topographies (Supplementary Fig. S1). It is notable that vinculin staining of adhesions indicates much larger adhesion in MSCs on NSQ50 compared to cells on planar or on SQ (Fig. 1A insets) with cells on SQ utilising a number of smaller adhesions.

MSC FOCAL ADHESION QUANTIFICATION AND FREQUENCY

Vinculin immunostaining was used to quantify focal adhesion lengths for MSCs grown on the Flat, NSQ50 and SQ topographies following the classification method described by Biggs et al. [2007]; focal complexes (FX) $> 2 \,\mu m$, focal adhesions (FA) $2-5 \,\mu m$, and super-mature adhesions (SMA) $> 5 \,\mu m$ [Biggs et al., 2007].

FA size was statistically significantly larger in MSCs on the NSQ50 than observed in cells on the SQ and Flat control topographies ($P < 0.05$). The average FA size between SQ and Flat was comparable

($P > 0.05$; Fig. 2A). Frequency distribution of FX in MSCs was low in all topographies but was decreased in cells on NSQ50 and SQ relative to Flat control. However, both nanotopographies supported more of the larger FA ($> 3 \,\mu m$) than the Flat control. FA distribution was decreased on flat and SQ as adhesion length increased, in contrast to NSQ50 with increased relative percentage of FAs larger than $5 \,\mu m$. Thus, the NSQ50 MSCs had the higher number of SMAs in comparison to MSCs on SQ and Flat. Overall, MSCs on NSQ50 had 1.5-fold ($P < 0.001$) more FAs of the larger size ($> 5 \,\mu m$) than MSCs on the flat and 1.3-fold higher than SQ ($P > 0.05$); MSCs on SQ have 1.2-fold more FAs of the larger size ($> 5 \,\mu m$) than Flat ($P > 0.05$) at this 3-day time point (Fig. 2B).

Cell–extracellular matrix interactions trigger cascades of signals via membrane proteins at points of adhesion that are transmitted through the cytoskeleton to the nucleus and determine stem cell homing, proliferation and differentiation processes [Xiao et al., 2002]. Cell adhesion analysis showed that whilst MSCs on SQ developed numerous, relatively small, adhesions, MSCs on NSQ50 displayed fewer, but critically, larger adhesions (Figs. 1A and 2). This finding is in agreement with Biggs et al. [2008, 2009] who showed that human osteoblasts require large adhesions as the cells differentiate towards bone.

INTRACELLULAR TENSION

It was recently shown that discrete geometric cues within the cell environment strongly influence the cell cytoskeleton and subsequently osteogenic differentiation via contraction leading to intracellular tension [Kilian et al., 2010]. To address this possibility in our system, we stained the cells with phospho (P)-myosin II light chain, involved in the stabilisation of myosin filaments responsible for cell contractility. MSCs cultured on the osteogenic nanotopography (NSQ50) exhibited a higher degree of contractility as levels of actomyosin expression increased in comparison to planar control and MSC retention (SQ) nanotopographies ($P < 0.001$) (Fig. 3A,B and Supplementary Fig. S2).
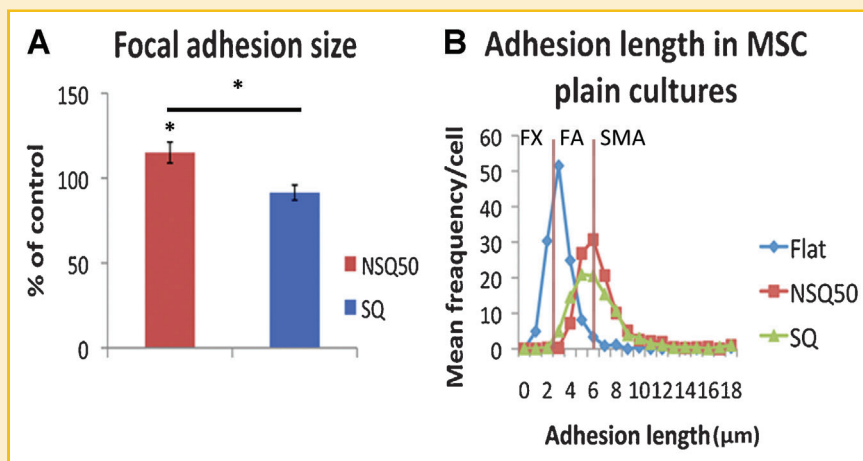

Fig. 2. Focal adhesion quantification. A: Graph showing FA mean length $\pm$ SD as % of control. B: Frequency distribution of different adhesion types in MSCs grown on the different nanotopographies. FX Frequency distribution in MSCs was decreased on NSQ50 and SQ relative to Flat control. FA distribution decreased as adhesion length increased on Flat and SQ but not so on NSQ50. The NSQ50 appeared to have the higher number of SMA in comparison to SQ and Flat. Comparison was done by ANOVA $^*P < 0.05$, $^{**}P < 0.01$, $^{***}P < 0.001$, n = 50. Note: markings above the error bars denote comparison to flat control; comparison between SQ and NSQ50 is denoted by a line.
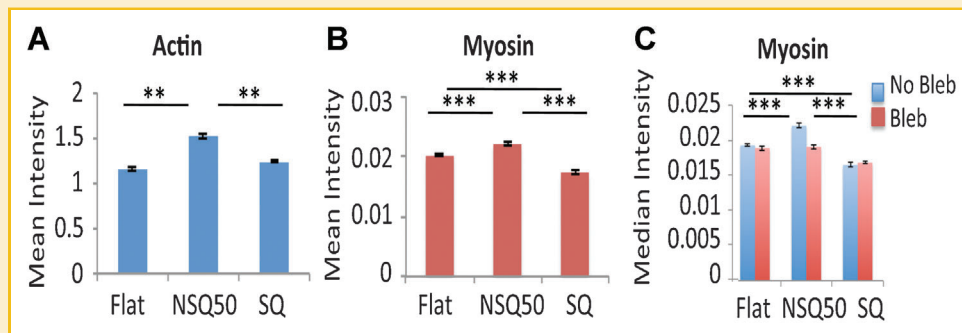
Fig. 3. Quantitative immunofluorescent results of MSCs grown on nanotopographies. In plain cultures, MSCs on NSQ demonstrate a higher degree of contractility in comparison to either SQ or the planar control ($P < 0.01$) with the highest actin (A) and myosin (B) intensities. C: In the presence of blebbistatin, a substantial decrease in P-myosin intensity is observed in NSQ indicating a high-tension state on this topography. Comparison by ANOVA $^*P < 0.05$, $^{**}P < 0.01$, $^{***}P < 0.001$, n = 900. Note: * above the error bars denote comparison to flat control; comparison between SQ and NSQ50 denoted by a line.

To further evaluate tension we assessed the effect of blebbistatin, known to modulate the cytoskeleton by inhibiting myosin II. The inhibitor was added to cell culture media at a concentration that allowed complete spreading of the MSC to the nanotopographies with no obvious changes in cell morphology (Supplementary Fig. S2). However, the shape of MSCs on NSQ50 appeared distorted, with the formation of stellate morphologies indicating release of a high degree of tension that the cells experience during osteogenesis (as confirmed by CellProfiler analysis in Fig. 3C and Supplementary Fig. S2) [Kamentsky et al., 2011].

The effects of cell cytoskeletal tension on stem cell differentiation were described by McBeath et al. [2004] and Kilian et al. [2010] with cells that were cultured on surfaces amenable to the formation of high tension developing organised actin filaments with large FAs in contrast to cells growing on surfaces that reduce intracellular tension which displayed a more relaxed cytoskeleton and smaller focal adhesions. In agreement with their studies where the authors showed that high tension was important to osteogenesis, we show indirectly and directly (myosin) that large adhesions and well-organised cytoskeleton result in MSCs cultured on NSQ50.

We next looked at a further cytoskeletal protein, vimentin. Vimentin has been considered in Ingber's tensegrity model to have a role in conveyance of mechanical signals to the nucleus as it forms a tension-bearing component of the tensegrity structure [Ingber, 2003a,b; Wang et al., 2009]. We note that both vimentin intermediate filaments and actin microfilaments directly connect to the nucleus via LINC complexes and microfilaments are also are under tension in the tensegrity model. Here, we used vimentin densitometry as an indicator of intracellular tensional differences between NSQ50 and SQ nanotopographies. Cells on the NSQ50 nanotopography showed a statistically significantly lower density of vimentin than the flat control ($P < 0.001$) and the SQ, indicating possible expansion due to applied tension (Supplementary Fig. S3).

NUCLEAR SHAPE AND LAMIN ORGANISATION

Lamins are nucleoskeletal intermediate filaments that are directly attached to the cytoskeleton through linker of nucleoskeleton and cytoskeleton (LINC) complexes [Ostlund et al., 2009]. Lamins are readily expanded by applied tension and it appears that the nucleus is designed to respond to intracellular tension (Fig 1D) [Dahl et al., 2004; Pajerowski et al., 2007]. Here we used lamin A/C (Fig. 4) and B (Supplementary Fig. S4) densitometry as an indirect indicator of changes in intracellular tension. MSCs on the NSQ50 surface display a statistically significantly lower density of lamin A/C network than the
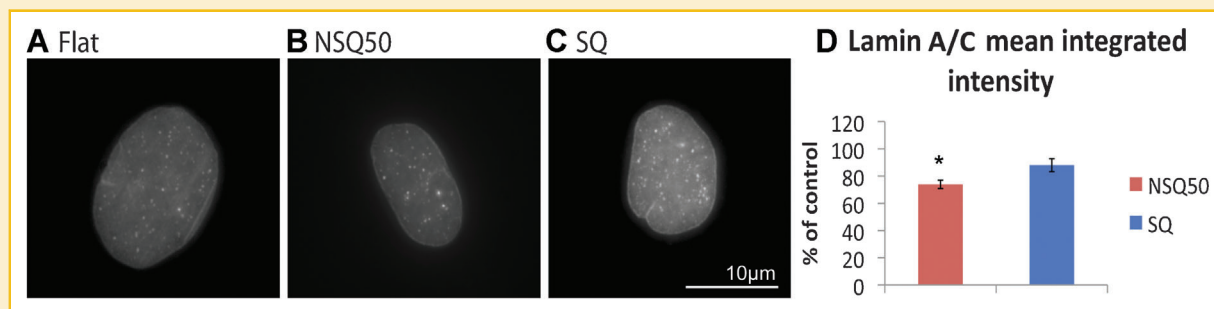

Fig. 4. Lamin A/C organization in MSC. Lamin A/C organisation images on the different nanotopographies (A) Flat, (B) NSQ50, (C) SQ. D: MSCs on the NSQ50 surface displayed a statistically significantly lower density of lamin A/C network than the Flat control ($P < 0.05$, ANOVA) indicating expansion due to applied tension. Graph shows mean integrated intensity $\pm$ SD as percentage of control, comparison by ANOVA $^*P < 0.05$, $^{**}P < 0.01$, $^{***}P < 0.001$, n = 45. Scale bar as indicated.

flat control ($P < 0.05$) indicating possible expansion due to applied tension (as cytoskeletal tension derived through large adhesion and well organised stress fibres is applied to the nucleus, the lamins would expand and density decrease). Similar results are obtained for MSCs for lamin B network (Supplementary Fig. S4).

Such lamina organisation could affect the nuclear compartmentalisation leading to repositioning of subnuclear components including chromosomes. We have previously shown using FISH for Ch1 that significant territory shifts are observed in cells on NSQ50 (high tension) from a more central location, euchromatic state, towards the periphery to a more quiescent heterochromatic state. In contrast, Ch1 territory positioning on SQ (low tension) topography was similar to the Flat control. Interestingly, Affymetrix array analysis identified Ch1 as the one with the highest number of differentially expressed genes that were generally mostly down-regulated. Assessment of chromosomal band positioning showed gain of down-regulations at the telomeric regions of both the q and p arm of the larger chromosomes in particular Ch1 [Tsimbouri et al., 2013]. We confirm this data in Supplementary Figure S5.

PHENOTYPE AND FUNCTION

Multiple important classes of differentially expressed genes that feed into major functional pathways were highlighted in the microarray data following Ingenuity Pathways Analysis. A number of these genes are relevant to the effects of mechanostimulation on the lamina and chromosomes through cellular remodelling (Fig. 5). More specifically, genes feeding into tissue development, cell cycle (Cyclin D, Mitogen activated protein 2 kinase 1/2 (MAP2k 1/2)), cell assembly and organization, DNA replication, recombination and repair, cell-to-cell signalling and interaction, cell signalling (bone morphogenetic protein (BMP) 2 signalling) and cell function and maintenance were

found to be predominantly up-regulated in the NSQ50 MSCs in comparison to those grown on the SQ nanotopography (example network shown in Supplementary Fig. S6). Whereas genes falling into pathways such as cell growth and proliferation, were observed to be predominantly down-regulated in the NSQ50 MSCs in comparison to those grown on the SQ nanotopography (example network shown in Supplementary Fig. S7) at this time point.

Interestingly, amino acid and protein synthesis signalling were also up-regulated on NSQ50 compared to SQ. This links well to metabolomics analysis where we found that MSCs on NSQ50 have enhanced up-regulations in such pathways illustrating again that actively differentiating cells are more metabolically active (Fig. 6 and Supplementary Fig. S8) [Reyes et al., 2006; Tsimbouri et al., 2012]. Lipid biosynthesis was found up-regulated on the SQ which can be related to energy requirements for cell self-renewal. Interestingly, we previously identified low-density lipoprotein (LDL) as potential major signalling hub involved in retention of multipotency [Tsimbouri et al., 2012]. We have also identified c-Jun N-terminal kinase (Jnk) as a signalling hub in self-renewal and here we decided to see if they may also be linked in the process of differentiation. We used a 3-day chemical inhibition of Jnk and antibody inhibition of the LDL receptor. Examination at the gene level using qRT-PCR, of the osteogenic marker runt-related transcription factor 2 (RUNX2) and chondrogenic marker SOX9 on treated samples compared to uninhibited planar control showed that expression of RUNX2 and SOX9 in MSCs on NSQ significantly reduced (Fig. 7). After 7 days of recovery from inhibition, SOX9 and RUNX2 were seen to increase in expression close to original levels (Fig. 7). These results indicate a possible role of JNK and LDL in not only retention of multipotency (as previously shown [Tsimbouri et al., 2012]) but also in MSC differentiation.
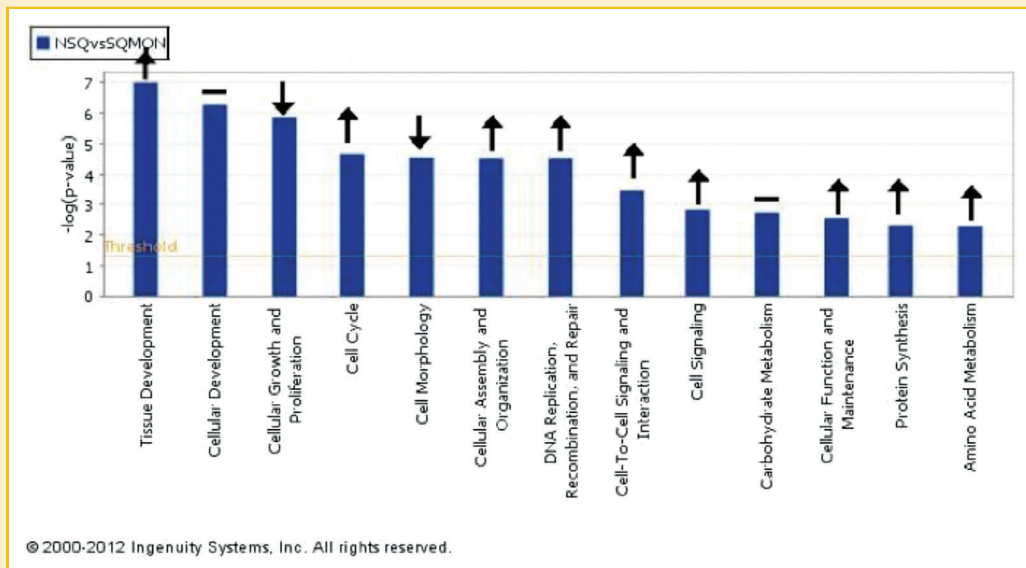
Fig. 5. Transcriptomic modulation in MSCs on NSQ50 versus SQ nanotopographies. Illustration of some functional classes of transcripts that are differentially expressed between cells cultured on the NSQ50 and SQ nanotopographies after they were normalised to the flat control. Applied thresholds are 1.4–fold change and $P < 0.05$ (Fisher's exact test n = 3 pairs of biological replicate arrays). ↑ indicates increased number of up–regulated genes on NSQ50 versus SQ. ↓ indicates more down–regulated genes on NSQ50 versus SQ and – indicates no change in gene expression between the topographies.
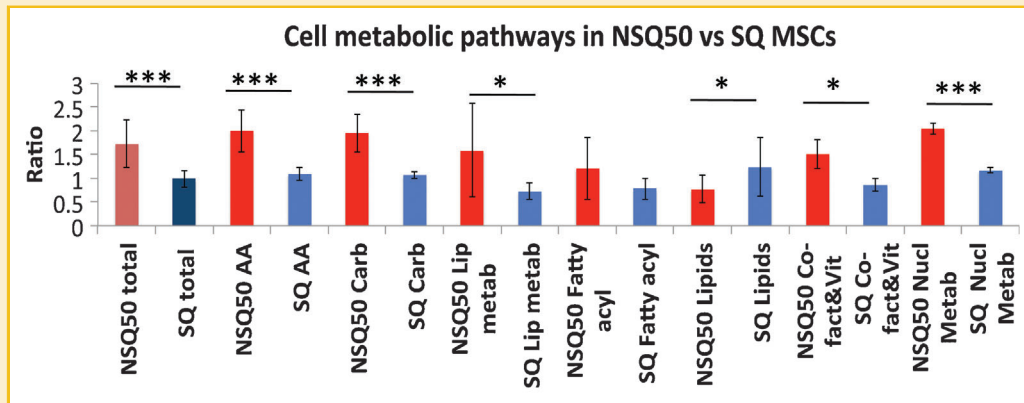
Fig. 6. Linking metabolism to phenotype. Total MSC metabolite values (up/down-regulations) derived from mass spectrometry data for metabolites after being normalized to flat control. Total cell metabolism is shown on darker colours and the different pathways in lighter equivalents. For SQ, the MSC retention surface, total metabolism is low. For NSQ50, the osteogenic surface, metabolism is statistically significantly higher than for MSCs cultured on SQ. The results seen for total metabolic activity can be reproduced when key cell activity pathways are focused upon such as amino acid (AA), Carbohydrate (Carb), lipid and nucleotide (Nucl) metabolism, fatty acyls and cofactors and vitamins (Co-fact&vit). In contrast, lipid biosynthesis was found statistically significantly higher in the SQ versus NSQ50. For metabolic analysis n = 3, results are the mean ± SD, statistics by t-test, $^*P < 0.05$, $^{**}P < 0.01$.

CHEMICAL PLASTICITY AND PHENOTYPE

As discussed, Yanes et al., have previously shown that embryonic stem cells contain large numbers of unsaturated metabolites and postulated that these are required for chemical plasticity. Using the SQ topography we have previously reported that similar metabolic profile is observed in MSCs with retained stem cell phenotype [McMurray et al., 2011]. As expected, differentiating MSCs on NSQ50 have a larger metabolite pool with fewer double carbon (CC) bonds compared to MSCs cultured on SQ. By determining the relative ratios for each metabolite, we calculated the metabolite abundance for cells cultured on the NSQ50 nanotopography relative to those cultured on the SQ. MSCs on the SQ nanotopography have a threefold higher CC bond content (0.52 vs. 1.61 CC per metabolite) than the MSCs grown on the NSQ50 (Fig. 8 and Supplementary Table I). Increased metabolic rate has been reported in differentiating MSCs grown in osteogenic media assessed by redox assays in which a decreased redox potential
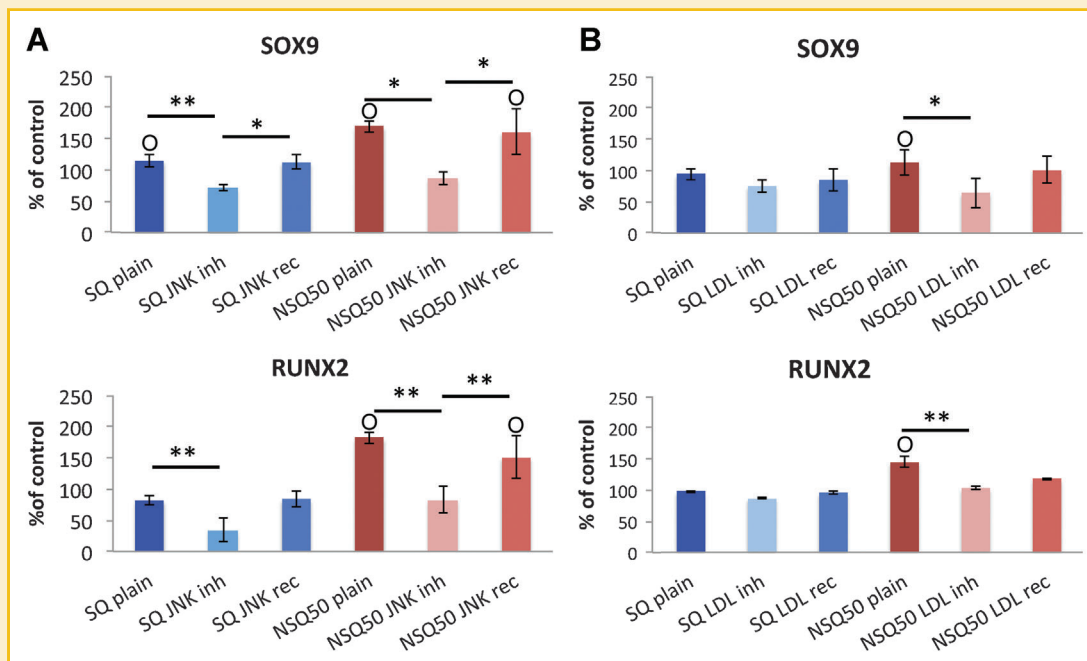

Fig. 7. JNK and LDL inhibition effects for MSCs on NSQ and SQ normalised to gene expression on planar control. A: For JNK inhibition a statistically significant reduction of the expression of osteogenic RUNX2 and chondrogenic SOX9 marker, was seen on both SQ and NSQ50. B: For the LDL receptor blocking significant down-regulation of both RUNX2 and SOX9, was noted on the NSQ50. As inhibition was ended for both JNK and LDL, RUNX2 and SOX9 expression was seen to increase and the difference to planar control become insignificant demonstrating recovery of differentiation. Results are mean ± SD for n = 9 material replicates, ANOVA $^*P < 0.05$, o = comparison to planar control, * = comparison between culture treatments.
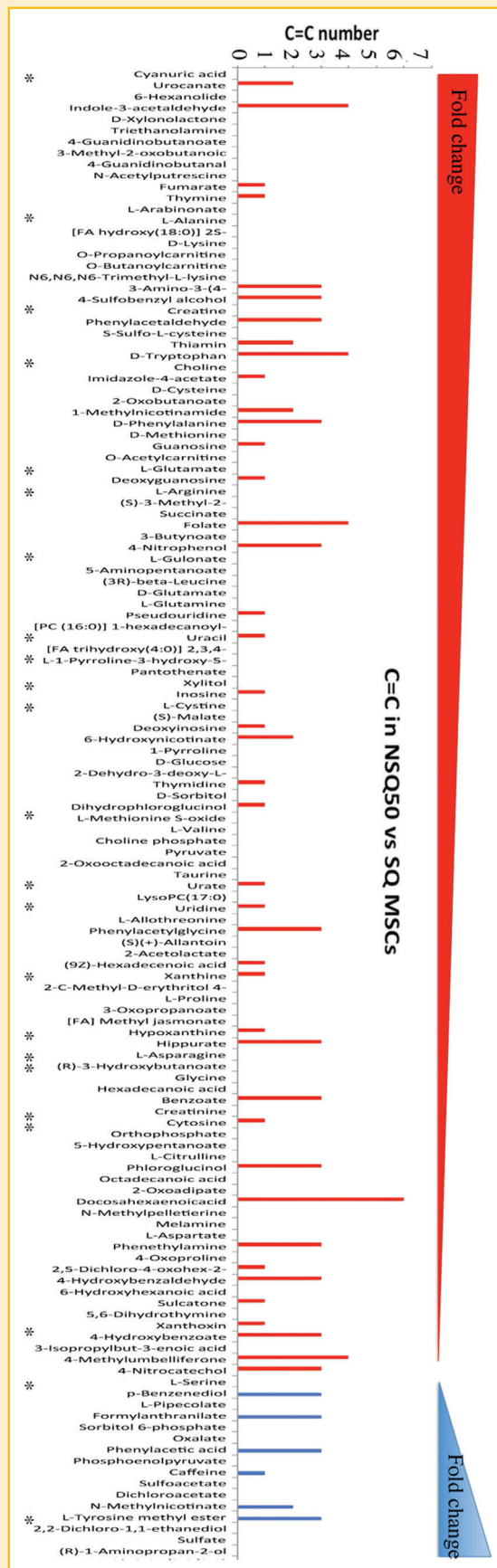
Fig. 8. Chemical unsaturations as detected by mass spectrometry. Metabolic saturation in MSCs cultured on NSQ50 versus SQ. Using the KEGG (Kyoto Encyclopedia of Genes and Genomes) ID for each metabolite the number of CC bonds was identified for each using the KEGG database. Initially, whilst more metabolites were identified in cells on NSQ50, they were largely saturated. However, in cells on SQ, fewer, but highly unsaturated, metabolites were detected. Validated metabolites are indicated by an asterisk.

of the cells as the cells differentiated was observed [Reyes et al., 2006]. Differentiated populations on NSQ50 showed increased levels of saturated free fatty acids together with their acyl-carnitine equivalents previously associated with bone marrow cell regeneration [Brohult, 1958]. Furthermore, saturated molecules involved in amino acid, carbohydrate, and nucleotide metabolism, processes important for the high energy demanding differentiation, were found prevalent in MSCs on the NSQ50 nanotopography.

However, metabolites on the SQ topography represented a pool of basal metabolites that with data analysis do not really 'pigeon-hole' well into functional requirements. We can thus speculate that these are perhaps not functional in themselves, but are perhaps useful to the cells to allow differentiation or proliferation upon demand. This fits well with the Yanes hypothesis that a pool of unsaturated metabolites give chemical plasticity to stem cells [Yanes et al., 2010].

CONCLUSIONS

We present a non-invasive, in vitro model system that can be used to study osteogenesis or/and self-renewal of MSCs. Analysis of the architectural and molecular effects of the two different nano-topographies on MSC morphology and phenotype indicate that the nuclear lamina is remodelled, with concomitant modulation of chromosomal positioning during osteogenesis but not self-renewal. Metabolic and pathway analysis of MSCs cultured on SQ nano-topography indicate that MSCs undergo down-regulation of canonical and metabolic signalling which result in reduced phenotypical change in contrast to MSCs on the NSQ50 nanotopography which undergo osteogenic differentiation. These studies offer new insight into the differentiation of stem cells on discrete nanotopographies indicating a complex interplay of metabolic, indirect and direct mechanotrans-duction in MSC phenotypical regulation.

ACKNOWLEDGEMENTS

REFERENCES

Biamonti G, Giacca M, Perini G, Contreas G, Zentilin L, Weighardt F, Guerra M, Della Valle G, Saccone S, Riva S. 1992. The gene for a novel human lamin maps at a highly transcribed locus of chromosome 19 which replicates at the onset of S-phase. Mol Cell Biol 12:3499–3506.

Biggs MJ, Richards RG, Gadegaard N, Wilkinson CD, Dalby MJ. 2007. Regulation of implant surface cell adhesion: Characterization and quantifica-tion of S-phase primary osteoblast adhesions on biomimetic nanoscale substrates. J Orthop Res 25:273–282.

Biggs MJ, Richards RG, McFarlane S, Wilkinson CD, Oreffo RO, Dalby MJ. 2008. Adhesion formation of primary human osteoblasts and the functional response of mesenchymal stem cells to 330 nm deep microgrooves. J R Soc Interface 5:1231–1242.

Biggs MJ, Richards RG, Gadegaard N, Wilkinson CD, Oreffo RO, Dalby MJ. 2009. The use of nanoscale topography to modulate the dynamics of adhesion formation in primary osteoblasts and ERK/MAPK signalling in STRO-1+ enriched skeletal stem cells. Biomaterials 30:5094–5103.

Brohult A. 1958. Effects of alkoxyglycerols and especially selachyl alcohol on the bone marrow in connexion with irradiation treatment and in leukaemia therapy. Nature 181:1484–1485.

Chen W, Villa-Diaz LG, Sun Y, Weng S, Kim JK, Lam RH, Han L, Fan R, Krebsbach PH, Fu J. 2012. Nanotopography influences adhesion, spreading, and self-renewal of human embryonic stem cells. ACS Nano 6:4094–4103.

Creek DJ, Jankevics A, Breitling R, Watson DG, Barrett MP, Burgess KE. 2011. Toward global metabolomics analysis with hydrophilic interaction liquid chromatography-mass spectrometry: Improved metabolite identification by retention time prediction. Anal Chem 83:8703–8710.

Creek DJ, Jankevics A, Burgess KE, Breitling R, Barrett MP. 2012. IDEOM: An Excel interface for analysis of LC-MS-based metabolomics data. Bioinformat-ics 28:1048–1049.

Dahl KN, Kahn SM, Wilson KL, Discher DE. 2004. The nuclear envelope lamina network has elasticity and a compressibility limit suggestive of a molecular shock absorber. J Cell Sci 117:4779–4786.

Dalby M, Riehle M, Johnstone H, Affrossman S, Curtis A. 2002. Polymer-demixed nanotopography: Control of fibroblast spreading and proliferation. IEEE Trans Nanobiosci 1:12–17.

Dalby MJ, Gadegaard N, Tare R, Andar A, Riehle MO, Herzyk P, Wilkinson CD, Oreffo RO. 2007. The control of human mesenchymal cell differentiation using nanoscale symmetry and disorder. Nat Mater 6:997–1003.

Diener A, Nebe B, Luthen F, Becker P, Beck U, Neumann HG, Rychly J. 2005. Control of focal adhesion dynamics by material surface characteristics. Biomaterials 26:383–392.

Engler AJ, Sen S, Sweeney HL, Discher DE. 2006. Matrix elasticity directs stem cell lineage specification. Cell 126:677–689.

Gadegaard N, Mosler S, Larsen NB. 2003. Biomimetic polymer nanostructures by injection moulding. Macromeolecular Mater Eng 288:76–83.

Gehrig K, Cornell RB, Ridgway ND. 2008. Expansion of the nucleoplasmic reticulum requires the coordinated activity of lamins and CTP: Phosphocholine cytidyltransferase alpha. Mol Biol Cell 19:237–247.

Gilbert PM, Havenstrite KL, Magnusson KE, Sacco A, Leonardi NA, Kraft P, Nguyen NK, Thrun S, Lutolf MP, Blau HM. 2010. Substrate elasticity regulates skeletal muscle stem cell self-renewal in culture. Science 329:1078–1081.

Ingber DE. 1997. Integrins, tensegrity, and mechanotransduction. Gravit Space Biol Bull 10:49–55.

Ingber DE. 2003a. Tensegrity I. Cell structure and hierarchical systems biology. J Cell Sci 116:1157–1173.

Ingber DE. 2003b. Tensegrity II. How structural networks influence cellular information processing networks. J Cell Sci 116:1397–1408.

Ji L, LaPointe VL, Evans ND, Stevens MM. 2012. Changes in embryonic stem cell colony morphology and early differentiation markers driven by colloidal crystal topographical cues. Eur Cell Mater 23:135–146.

Kamentsky L, Jones TR, Fraser A, Bray MA, Logan DJ, Madden KL, Ljosa V, Rueden C, Eliceiri KW, Carpenter AE. 2011. Improved structure, function and compatibility for CellProfiler: Modular high-throughput image analysis software. Bioinformatics 27:1179–1180.

Kilian KA, Bugarija B, Lahn BT, Mrksich M. 2010. Geometric cues for directing the differentiation of mesenchymal stem cells. Proc Natl Acad Sci USA 107:4872–4877.

Lin F, Worman HJ. 1993. Structural organization of the human gene encoding nuclear lamin A and nuclear lamin C. J Biol Chem 268:16321–16326.

Lin F, Worman H. 1995. Structural organization of the human gene (LMNB1) encoding nuclear lamin B1. Genomics 27:230–236.

McBeath R, Pirone DM, Nelson CM, Bhadriraju K, Chen CS. 2004. Cell shape, cytoskeletal tension, and RhoA regulate stem cell lineage commitment. Dev Cell 6:483–495.

McMurray RJ, Gadegaard N, Tsimbouri PM, Burgess KV, McNamara LE, Tare R, Murawski K, Kingham E, Oreffo RO, Dalby MJ. 2011. Nanoscale surfaces for the long-term maintenance of mesenchymal stem cell phenotype and multipotency. Nat Mater 10:637–644.

McNamara LE, Sjostrom T, Burgess KE, Kim JJ, Liu E, Gordonov S, Moghe PV, Meek RM, Oreffo RO, Su B, Dalby MJ. 2011. Skeletal stem cell physiology on functionally distinct titania nanotopographies. Biomaterials 32:7403–7410.

Moir RD, Montag-Lowy M, Goldman RD. 1994. Dynamic properties of nuclear lamins: Lamin B is associated with sites of DNA replication. J Cell Biol 125:1201–1212.

Moir RD, Spann TP, Herrmann H, Goldman RD. 2000. Disruption of nuclear lamin organization blocks the elongation phase of DNA replication. J Cell Biol 149:1179–1192.

Muraglia A, Cancedda R, Quarto R. 2000. Clonal mesenchymal progenitors from human bone marrow differentiate in vitro according to a hierarchical model. J Cell Sci 113(Pt7):1161–1166.

Narita Y, Yamawaki A, Kagami H, Ueda M, Ueda Y. 2008. Effects of transforming growth factor-beta 1 and ascorbic acid on differentiation of human bone-marrow-derived mesenchymal stem cells into smooth muscle cell lineage. Cell Tissue Res 333:449–459.

Oh S, Brammer KS, Li YSJ, Teng D, Engler AJ, Chien S, Jin S. 2009. Stem cell fate dictated solely by altered nanotube dimension. Proc Natl Acad Sci USA 106:2130–2135.

Ostlund C, Folker ES, Choi JC, Gomes ER, Gundersen GG, Worman HJ. 2009. Dynamics and molecular interactions of linker of nucleoskeleton and cytoskeleton (LINC) complex proteins. J Cell Sci 122:4099–4108.

Pajerowski JD, Dahl KN, Zhong FL, Sammak PJ, Discher DE. 2007. Physical plasticity of the nucleus in stem cell differentiation. Proc Natl Acad Sci USA 104:15619–15624.

Park DW, Park KH, Lee JW, Hwang KJ, Choi YK. 2007. Hydrochloric acid treatment of TiO_2 electrode for quasi-solid-state dye-sensitized solar cells. J Nanosci Nanotechnol 7:3722–3726.

Pittenger MF, Mackay AM, Beck SC, Jaiswal RK, Douglas R, Mosca JD, Moorman MA, Simonetti DW, Craig S, Marshak DR. 1999. Multilineage potential of adult human mesenchymal stem cells. Science 284:143–147.

Reyes JM, Fermanian S, Yang F, Zhou SY, Herretes S, Murphy DB, Elisseeff JH, Chuck RS. 2006. Metabolic changes in mesenchymal stem cells in osteogenic medium measured by autofluorescence spectroscopy. Stem Cells 24:1213–1217.

Scheltema RA, Jankevics A, Jansen RC, Swertz MA, Breitling R. 2011. PeakML/mzMatch: A file format, Java library, R library, and tool-chain for mass spectrometry data analysis. Anal Chem 83:2786–2793.

Smith CA, Want EJ, O'Maille G, Abagyan R, Siuzdak G. 2006. XCMS: Processing mass spectrometry data for metabolite profiling using nonlinear peak alignment, matching, and identification. Anal Chem 78:779–787.

Thomas TE, Abraham SJ, Lansdorp PM. 2002. Flow cytometry and immunoselection of human stem cells. Methods Mol Med 63:29–57.

Treiser MD, Yang EH, Gordonov S, Cohen DM, Androulakis IP, Kohn J, Chen CS, Moghe PV. 2010. Cytoskeleton-based forecasting of stem cell lineage fates. Proc Natl Acad Sci USA 107:610–615.

Tsimbouri PM, McMurray RJ, Burgess KV, Alakpa EV, Reynolds PM, Murawski K, Kingham E, Oreffo RO, Gadegaard N, Dalby MJ. 2012. Using nano-topography and metabolomics to identify biochemical effectors of multi-potency. ACS Nano 6:10239–10249.

Tsimbouri PM, Murawski K, Hamilton G, Herzyk P, Oreffo RO, Gadegaard N, Dalby MJ. 2013. A genomics approach in determining nanotopographical effects on MSC phenotype. Biomaterials 34:2177–2184.

Wang N, Butler JP, Ingber DE. 1993. Mechanotransduction across the cell surface and through the cytoskeleton. Science 260:1124–1127.

Wang N, Tytell JD, Ingber DE. 2009. Mechanotransduction at a distance: Mechanically coupling the extracellular matrix with the nucleus. Nat Rev Mol Cell Biol 10:75–82.

Wood MA, Bagnaninchi P, Dalby MJ. 2008. The beta integrins and cytoskeletal nanoimprinting. Exp Cell Res 314:927–935.

Wozniak MA, Modzelewska K, Kwong L, Keely PJ. 2004. Focal adhesion regulation of cell behavior. Biochim Biophys Acta 1692:103–119.

Xiao G, Jiang D, Gopalakrishnan R, Franceschi RT. 2002. Fibroblast growth factor 2 induction of the osteocalcin gene requires MAPK activity and phosphorylation of the osteoblast transcription factor, Cbfa1/Runx2. J Biol Chem 277:36181–36187.

Yanes O, Clark J, Wong DM, Patti GJ, Sanchez-Ruiz A, Benton HP, Trauger SA, Desponts C, Ding S, Siuzdak G. 2010. Metabolic oxidation regulates embryonic stem cell differentiation. Nat Chem Biol 6:411–417.

Yim EK, Pang SW, Leong KW. 2007. Synthetic nanostructures inducing differentiation of human mesenchymal stem cells into neuronal lineage. Exp Cell Res 313:1820–1829.

SUPPORTING INFORMATION

Additional supporting information may be found in the online version of this article at the publisher's web-site.